Yamamoto Y, Hiasa Y, Murakami H, Ikeda Y, Yamanishi H, Abe M, Matsuura B, Onji M.	Rapid alternative absorption of dietary long-chain fatty acids with upregulation of intestinal glycosylated CD36 in liver cirrhosis.	Am J Clin Nutr	96	90-101	2012
Ochi H, Hirooka M, Koizumi Y, Miyake T, Tokumoto Y, Soga Y, Tada F, Abe M, Hiasa Y, Onji M.	Real-time tissue elastography for evaluation of hepatic fibrosis and portal hypertension in nonalcoholic fatty liver diseases.	Hepatology	56	1271-8	2012
Takeji S, Hirooka M, Koizumi Y, Tokumoto Y, Abe M, Ikeda Y, Nadano S, Hiasa Y, Onji M.	Des-gamma-carboxy prothrombin identified by P-11 and P-16 antibodies reflects prognosis for patients with hepatocellular carcinoma.	J Gastroenterol Hepatol.	E-pub		2012
Kuno A, Ikehara Y, Tanaka Y, Ito K, Matsuda A, Sekiya S, Hige S, Sakamoto M, Kage M, Mizokami M, Narimatsu H.	A serum "sweet-doughnut" protein facilitates fibrosis evaluation and therapy assessment in patients with viral hepatitis.	Sci Rep.	3	1065	2013
Fukuma M, Tanese K, Effendi K, Yamazaki K, Masugi Y, Suda M, Sakamoto M.	Leucine-rich repeat-containing G protein-coupled receptor 5 regulates epithelial cell phenotype and survival of hepatocellular carcinoma cells.	Exp Cell Res.	319 (3)	113-21	2013
Effendi K, Yamazaki K, Mori T, Masugi Y, Makino S, Sakamoto M.	Involvement of hepatocellular carcinoma biomarker, cyclase-associated protein 2 in zebrafish body development and	Exp Cell Res.	319 (1)	35-44.	2013
Reiichiro Kondo, et al	Accumulation of platelets in the liver may be an important contributory factor to thrombocytopenia and liver fibrosis in chronic hepatitis C	J Gastroenterol	DOI 10.1007/s 00535-01 2-0656-2		2012

Ⅳ. 研究成果の刊行物・別刷

Oncology

Oncology 2013;84(suppl 1):13–20
DOI: 10.1159/000345884

Published online: February 20, 2013

Assessment of Liver Fibrosis with Real-Time Tissue Elastography in Chronic Viral Hepatitis

Norihisa Yada[a] Masatoshi Kudo[a] Hiroyasu Morikawa[b] Kenji Fujimoto[c, d] Michio Kato[d] Norifumi Kawada[b]

[a]Department of Gastroenterology and Hepatology, Kinki University Faculty of Medicine, Osakasayama, [b]Department of Hepatology, Graduate School of Medicine, Osaka City University, Osaka, and [c]Division of Clinical Research and [d]Department of Internal Medicine, National Hospital Organization, Minamiwakayama Medical Center, Tanabe, Japan

Key Words

Real-time tissue elastography · FibroScan · Liver fibrosis · Liver stiffness

Abstract

Objective: The aim of this study was to assess prospectively the accuracy of measurement of liver fibrosis with real-time tissue elastography (RTE) in patients with chronic viral hepatitis. ***Methods:*** Two hundred and forty-five patients were prospectively enrolled. Nine image features were measured from strain images, and Liver Fibrosis Index (LFI) was calculated from these features. Fibrosis stage was diagnosed from pathological specimens obtained by ultrasound-guided biopsy. LFI and serological markers were compared with pathological diagnosis, and the diagnostic performance of RTE was compared. ***Results:*** LFI in stages F0–F1, F2, F3 and F4 was 1.58, 2.03, 2.40 and 2.86, respectively, demonstrating a stepwise increase with increasing severity of liver fibrosis ($p < 0.001$). LFI in F2 did not significantly differ from that in F3, whereas for all other combinations of stages, there were significant differences. The area under the receiver operating characteristic curve of the LFI, platelet count, aspartate/alanine aminotransferase ratio, aspartate aminotransferase-to-platelet ratio, and FibroIndex for predicting F3 stage or higher (F0–F2 vs. F3–F4) was 0.865, 0.824, 0.708, 0.789 and 0.828, respectively. ***Conclusions:*** RTE is useful for diagnosis of liver fibrosis, regardless of stage, in patients with chronic viral hepatitis.

Introduction

The assessment of liver fibrosis is an important factor in deciding on therapeutic options and for predicting the prognosis of chronic hepatitis. Biopsy is the gold standard for assessment of liver fibrosis; however, it carries risks such as bleeding and pain. Furthermore, needle biopsy of the liver has been shown to be associated with a high rate of sampling error in patients with diffuse parenchymal liver diseases. The possibility of sampling error with liver biopsy arises because the tissue obtained represents only a small portion (approx. one part in 50,000) of the entire liver mass [1–3].

Elastography is reported to be useful for diagnosis of liver fibrosis and has a variety of measurement methods [4, 5]. FibroScan, virtual-touch tissue quantification, and shear wave elastography measure the propagation speed

KARGER

Fax +41 61 306 12 34
E-Mail karger@karger.com
www.karger.com

0030–2414/13/0847–0013$38.00/0

Accessible online at:
www.karger.com/ocl

Masatoshi Kudo, MD, PhD
Division of Gastroenterology and Hepatology, Department of Internal Medicine
Kinki University Faculty of Medicine
377-2 Ohno-Higashi, Osakasayama, Osaka 589-8511 (Japan)
E-Mail m-kudo@med.kindai.ac.jp

of the shear wave [6–8]. The more severe hepatic fibrosis progresses, the faster propagation speed increases. They are said to be useful for the diagnosis of liver fibrosis, especially in advanced fibrosis cases. However, the propagation speed of the shear wave is not only affected by liver fibrosis, but also hepatic activity, jaundice and hepatic congestion [9–12]. The other method measures tissue distortion. Real-time tissue elastography (RTE) shows in real time the strain of the tissue. It has been reported that RTE is useful for evaluation of malignant tumors in the mammary gland and thyroid [13, 14].

In the present study, we investigated the performance of RTE for diagnosis of liver fibrosis. We also compared the diagnostic performance of RTE and serum markers of fibrosis.

Patients and Methods

Patients

This was a multicenter, cross-sectional study that was performed at Kinki University Hospital (Osaka, Japan), Osaka City University Hospital (Osaka, Japan) and Minamiwakayama Medical Center (Wakayama, Japan). Consecutive patients with chronic hepatitis C virus (HCV) or chronic by hepatitis B virus (HBV) infection, who underwent percutaneous ultrasound-guided liver biopsy before treatment, were enrolled. Only patients with HCV or HBV, whose disease was defined by the presence of serum anti-HCV antibody and serum HCV RNA, or the presence of serum hepatitis B surface antibody and serum HBV DNA, were included. Percutaneous ultrasound-guided liver biopsy was performed within 2 weeks before or after RTE. Clinical and laboratory data were collected at the time of liver biopsy. Patients were excluded if they consumed >20 g alcohol per day. Patients with a history of autoimmune hepatitis, primary biliary hepatitis, primary sclerosing cholangitis, hemochromatosis, α1-antitrypsin deficiency, or Wilson's disease were also excluded. The study protocol conformed to the Declaration of Helsinki and was approved by the local ethics committee. Informed consent to participate in the study was obtained from each patient.

Clinical and Laboratory Assessments

Relevant clinical data recorded were age, sex, weight, height, waist circumference and cause of chronic liver disease. Body Mass Index was calculated as weight (kg) divided by height (m) squared. Blood samples were taken after overnight fasting on the day of biopsy. Laboratory tests including platelet count, cholesterol, bilirubin, aspartate aminotransferase (AST), alanine aminotransferase (ALT), γ-glutamyl transpeptidase, bilirubin, albumin, γ-globulins, prothrombin time and international normalized ratio were assessed using automated methods. From these single variables, three ratio indexes were calculated using classical ratios: AST/ALT [15]; AST-to-platelet ratio index [APRI; AST/upper limit of normal 100/platelet count (10^4/mm^3)] [16], and FibroIndex [1.738 – 0.064 × platelet count (10^4/mm^3) + 0.005 × AST (U/l) + 0.463 × γ-globulin (g/dl)] [17].

Liver Histological Assessment

Percutaneous ultrasound-guided liver biopsy was performed on the liver right lobe with a Tru-Cut semiautomatic 18-gauge needle apparatus (Monopty; C.R. Bard, Tempe, Ariz., USA). The liver biopsy specimens were fixed in formalin, embedded in paraffin and stained with hematoxylin and eosin, Masson's trichrome or Azan stain. All biopsy specimens were examined by pathologists who were blinded to the patient characteristics. Liver fibrosis was scored by the New Inuyama classification. The stage of fibrosis was classified from F0 to F4 as follows: F0, no fibrosis; F1, fibrosis portal expansion; F2, bridging fibrosis (portal–portal or portal–central linkage); F3, bridging fibrosis with lobular distortion (disorganization), and F4, cirrhosis.

Real-Time Tissue Elastography

RTE was performed using ultrasonography (EUS-8500, HI-VISION 900 and HI-VISION Ascendus; Hitachi Aloka Medical, Tokyo, Japan) and the EUP-L52 linear probe (3–7 MHz; Hitachi Aloka Medical). Patients were examined in the spine position with the right arm in maximal abduction and were instructed to hold their breath. The examinations were performed on the right lobe of the liver through the intercostal spaces, holding firmly the transducer without applying compression on the skin. The B-mode and static image superimposed on B-mode were both visualized in real-time; therefore, the best position could be easily selected. The region of interest (ROI) of the strain image was 2.5 cm^2 and located about 1 cm below the surface of the liver. In addition, to obtain good images, scanning was performed to avoid large vessels and attenuation by lungs and ribs. RTE shows a relative strain image, thus, there should be no artifacts in the ROI of the strain image.

Nine image features were extracted from each RTE image: mean relative strain value (MEAN); standard deviation of relative strain value (SD); percentage of low strain area (percentage of blue color area – %AREA); complexity of low strain area (calculated as perimeter^2/area – COMP); skewness (SKEW); kurtosis (KURT); entropy (ENT); textural complexity, inverse difference moment (IDM), and angular second moment (ASM). For stable extracting of image features, the extraction area approximately matched or was slightly smaller than the ROI of the strain image (fig. 1). To perform a quantitative evaluation, Liver Fibrosis Index (LFI) was calculated as follows: –0.009 × MEAN – 0.005 × SD + 0.023 × %AREA + 0.025 × COMP + 0.775 × SKEW – 0.281 × KURT + 2.083 × ENT + 3.042 × IDM + 39.979 × ASM – 5.542 [18, 19]. The median LFI was calculated from 10 images.

Statistical Analysis

Descriptive statistics are shown as the mean ± SD, median or percentage, as appropriate. Comparisons between groups were determined by Wilcoxon's signed rank test and confirmed by the nonparametric Mann-Whitney U test between groups. Correlation between data was tested using the nonparametric Spearman rank correlation analysis. Differences were considered statistically significant at $p < 0.05$. Tukey's Honestly Significant Difference test was used to compare the data among each fibrosis stage of chronic hepatitis. The diagnostic performance for liver fibrosis was determined in terms of sensitivity, specificity, positive predictive value, negative predictive value, diagnostic accuracy and area under the receiver operating characteristic curve (AUROC). Analysis was performed using SPSS Statistics 20 (IBM, Armonk, N.Y., USA).

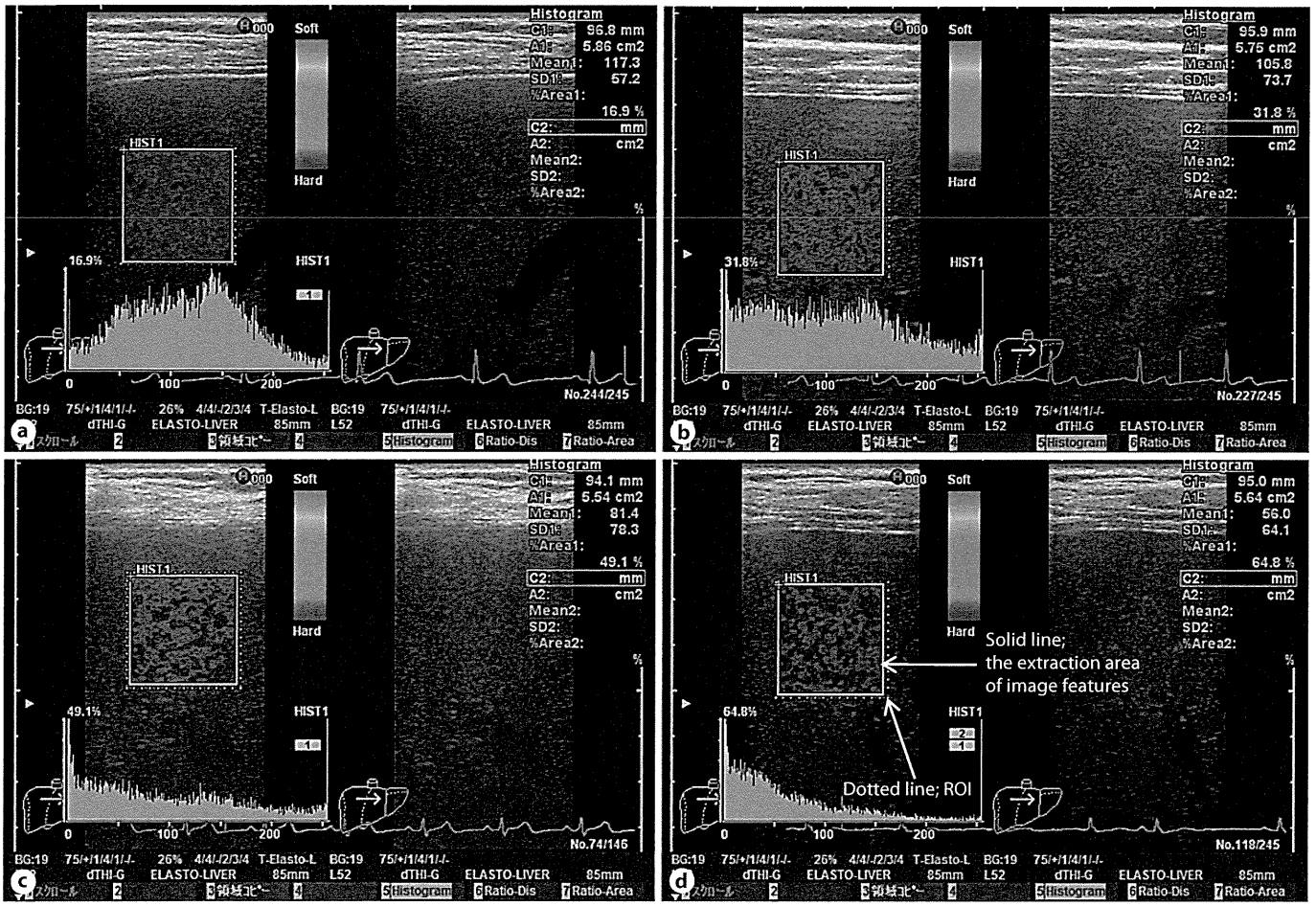

Fig. 1. RTE images in patients with chronic viral hepatitis. With fibrosis associated to progress, strain elastogram increases color variation between relatively low strain regions and generates a patched image pattern. F1 stage (**a**), F2 stage (**b**), F3 stage (**c**), F4 stage (**d**).

Results

Demographics and Baseline Features

In 4 patients, the liver biopsy specimen was too small to be used for pathological diagnosis. The remaining 245 patients, 137 (56.1%) men and 108 women (43.9%) who met the requirements were enrolled in the study. The clinical characteristics and laboratory data are shown in table 1. One hundred and eighty-nine patients (77.1%) had HCV and the other 56 (22.9%) had HBV. Four, 95, 77, 27 and 42 patients were respectively diagnosed with stage F0, F1, F2, F3 and F4 fibrosis. AST and alkaline phosphatase were significantly elevated with increasing severity of fibrosis ($p < 0.001$). Serum albumin, cholinesterase, total cholesterol, prothrombin time and platelet count were significantly decreased with increasing severity of fibrosis ($p < 0.001$).

Comparison of Serological Markers and Pathological Diagnosis

Serological fibrosis makers, platelet count, AST/ALT ratio, APRI and FibroIndex were compared with the pathological diagnosis of hepatic fibrosis. Platelet count in patients with F0–F1, F2, F3 and F4 stage fibrosis was 21.0, 15.7, 14.1 and 10.6 $\times$ $10^4/mm^3$, respectively, demonstrating a stepwise decrease with increasing severity of liver fibrosis ($p < 0.001$). AST/ALT ratio in patients with F0–F1, F2, F3 and F4 stage fibrosis was 1.09, 1.01, 1.59 and 1.33, respectively, and showed a slightly upward trend with increasing severity of liver fibrosis ($p = 0.001$). APRI in patients with F0–F1, F2, F3, and F4 stage fibrosis was 5.49, 11.37, 12.52 and 23.79, respectively, and FibroIndex in patients with F0–F1, F2, F3 and F4 stage was 1.21, 1.78, 1.82, and 2.31, respectively. Both APRI and FibroIndex

Table 1. Clinical characteristics and laboratory data of patients

Fibrosis stage	F0–F1	F2	F3	F4	Total	p value
Etiology (HCV/HBV)	70/30	63/16	20/7	39/3	189/56	
Sex (male/female)	55/44	45/32	15/12	22/20	137/108	
Age, years	51.4 ± 12.8	59.6 ± 14.0	59.6 ± 14.9	66.7 ± 11.6	57.7 ± 14.3	<0.001
Height, m	162.1 ± 8.2	165.3 ± 8.7	161.5 ± 7.5	160.1 ± 9.2	162.5 ± 8.4	NS
Weight, kg	60.7 ± 10.9	65.5 ± 14.7	59.4 ± 9.4	61.2 ± 14.2	61.7 ± 12.1	NS
Waist circumference, cm	82.8 ± 8.6	90.1 ± 14.1	87.9 ± 12.4	87.2 ± 10.6	85.7 ± 10.6	NS
Body mass index	23.1 ± 3.5	23.8 ± 4.2	22.8 ± 3.5	23.6 ± 3.7	23.3 ± 3.7	NS
AST, IU/l	43.6 ± 33.8	58.3 ± 48.2	63.3 ± 42.2	70.0 ± 47.2	54.0 ± 41.8	<0.001
ALT, IU/l	57.0 ± 63.3	69.6 ± 55.7	57.6 ± 46.7	59.7 ± 45.3	60.1 ± 56.6	NS
GGT, IU/l	42.3 ± 48.8	62.1 ± 70.1	45.2 ± 44.2	61.8 ± 86.6	50.4 ± 62.2	NS
ALP, IU/l	238.2 ± 83.4	266.6 ± 95.3	307.0 ± 169.8	376.7 ± 209.5	280.4 ± 141.4	<0.001
Total bilirubin, mg/dl	0.72 ± 0.49	0.92 ± 1.48	0.78 ± 0.58	1.09 ± 0.63	0.84 ± 0.82	<0.001
Total protein, g/dl	7.8 ± 7.1	7.2 ± 0.7	7.1 ± 0.9	7.1 ± 0.8	7.5 ± 4.9	NS
Serum albumin, g/dl	4.2 ± 0.4	4.1 ± 0.4	4.1 ± 0.7	3.6 ± 0.6	4.1 ± 0.5	<0.001
Gamma globulin, g/dl	1.4 ± 0.4	1.6 ± 0.4	1.7 ± 0.5	2.0 ± 0.5	1.6 ± 0.5	<0.001
Cholinesterase, IU/l	353.9 ± 99.8	288.3 ± 47.4	273.9 ± 76.5	157.4 ± 80.0	313.8 ± 105.0	<0.001
Total cholesterol, mg/dl	185.3 ± 32.7	172.2 ± 31.2	161.5 ± 34.9	149.7 ± 26.8	172.8 ± 34.4	<0.001
Prothrombin time, %	100.4 ± 11.7	95.8 ± 15.6	89.1 ± 14.9	76.6 ± 15.4	93.2 ± 16.4	<0.001
Platelets, $10^4/mm^3$	21.0 ± 6.0	15.7 ± 5.0	14.1 ± 4.7	10.6 ± 7.5	17.1 ± 7.3	<0.001
AST/ALT ratio	1.09 ± 0.92	1.01 ± 0.45	1.59 ± 1.46	1.33 ± 0.53	1.18 ± 0.88	0.001
APRI	5.49 ± 4.14	11.37 ± 13.68	12.52 ± 7.87	23.79 ± 26.23	11.05 ± 15.14	<0.001
FibroIndex	1.21 ± 0.45	1.78 ± 0.60	1.82 ± 0.55	2.31 ± 0.66	1.63 ± 0.70	<0.001
LFI	1.58 ± 0.67	2.03 ± 0.71	2.40 ± 0.64	2.86 ± 0.64	2.02 ± 0.82	<0.001
Total, n	99	77	27	42	245	

GGT = γ-Glutamyl transpeptidase; ALP = alkaline phosphatase.

showed a significant stepwise increase with severity of liver fibrosis ($p < 0.001$). However, there were a number of outliers in these serological markers (fig. 2).

Comparison between each F stage group was performed. Platelet count showed a significant decrease with severity of liver fibrosis between F0–F1 and F2, F0–F1 and F3, F0–F1 and F4, and F2 and F4. APRI showed a significant increase with severity of liver fibrosis between F0–F1 and F4, F2 and F4, and F3 and F4. FibroIndex showed a significant increase with severity of liver fibrosis between F0–F1 and F2, F0–F1 and F3, F0–F1 and F4, F2 and F4, and F3 and F4 (fig. 2).

Relationship between LFI and Pathological Liver Fibrosis

RTE was performed in all the enrolled patients. LFI was calculated as the median from 10 images. The median LFI in patients with F0–F1, F2, F3 and F4 stage fibrosis was 1.58, 2.03, 2.40 and 2.86, respectively, demonstrating a stepwise increase with increasing severity of liver fibrosis ($p < 0.001$). Comparison between each F stage group was performed. There was a significant increase between F0–F1 and F2, F0–F1 and F3, F0–F1 and F4, F2 and F4, and F3 and F4. The best cutoff of LFI for diagnosis of F2 or higher stage fibrosis (differentiating F2–F4 from F0–F1) was 2.05, and the accuracy was 73.0%. The best cutoff of LFI for diagnosis of F3 or higher stage fibrosis (differentiating F3–F4 from F0–F2) was 2.28, and the accuracy was 79.6%. The best cutoff of LFI for diagnosis of F4 stage fibrosis (differentiating F4 from F0–F3) was 2.36, and the accuracy was 78.3 (table 2).

Correlation with LFI and Serum Markers

The AUROC of the LFI, platelet count, AST/ALT ratio, APRI and FibroIndex for predicting F2 or higher stage fibrosis (F0–F1 vs. F2–F4) was 0.800, 0.832, 0.646, 0.820 and 0.853, respectively. Similarly, the AUROC for predicting F3 or higher stage fibrosis (F0–F2 vs. F3–F4) was 0.865, 0.824, 0.708, 0.789 and 0.828, respectively.

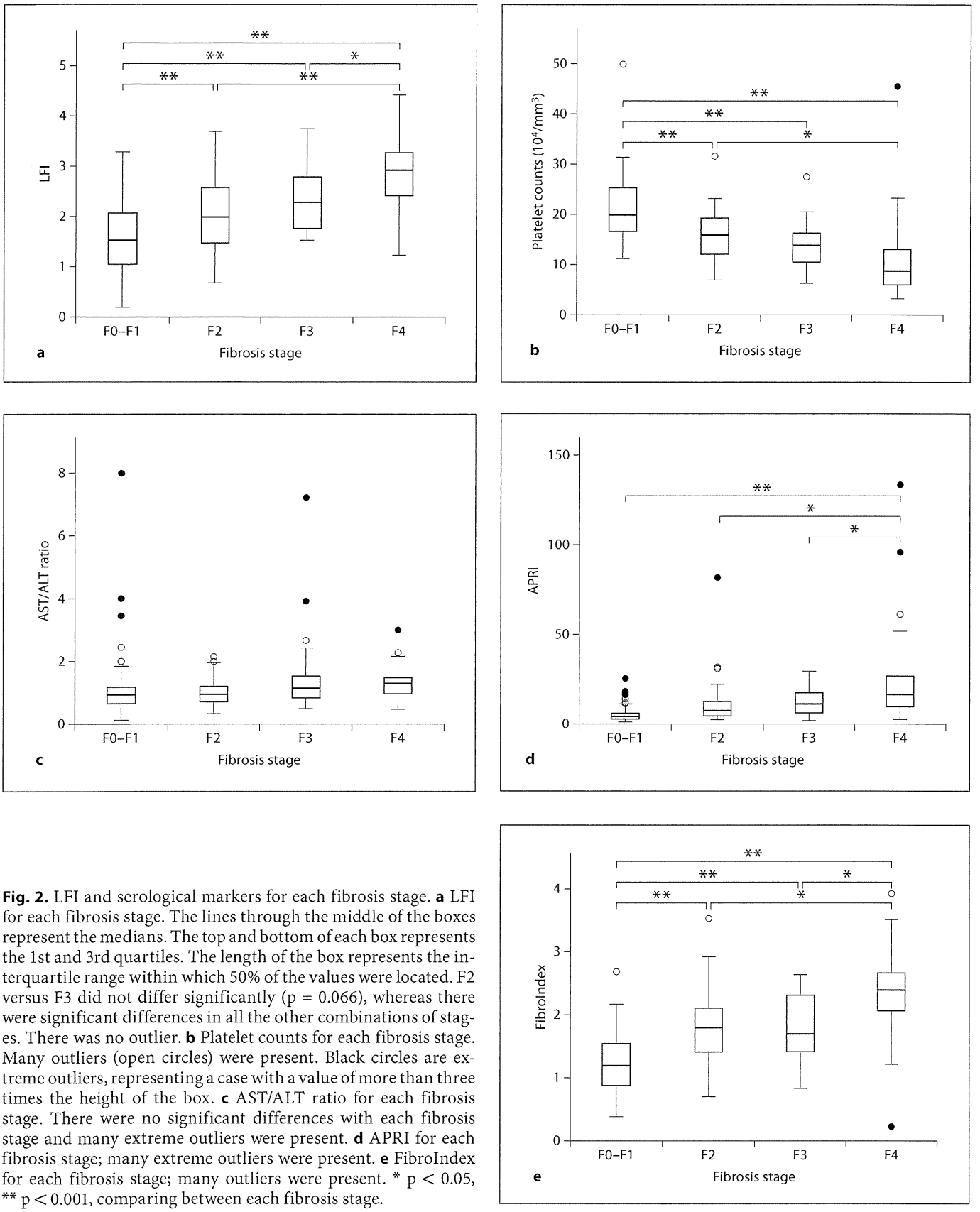

Fig. 2. LFI and serological markers for each fibrosis stage. **a** LFI for each fibrosis stage. The lines through the middle of the boxes represent the medians. The top and bottom of each box represents the 1st and 3rd quartiles. The length of the box represents the interquartile range within which 50% of the values were located. F2 versus F3 did not differ significantly ($p = 0.066$), whereas there were significant differences in all the other combinations of stages. There was no outlier. **b** Platelet counts for each fibrosis stage. Many outliers (open circles) were present. Black circles are extreme outliers, representing a case with a value of more than three times the height of the box. **c** AST/ALT ratio for each fibrosis stage. There were no significant differences with each fibrosis stage and many extreme outliers were present. **d** APRI for each fibrosis stage; many extreme outliers were present. **e** FibroIndex for each fibrosis stage; many outliers were present. * $p < 0.05$, ** $p < 0.001$, comparing between each fibrosis stage.

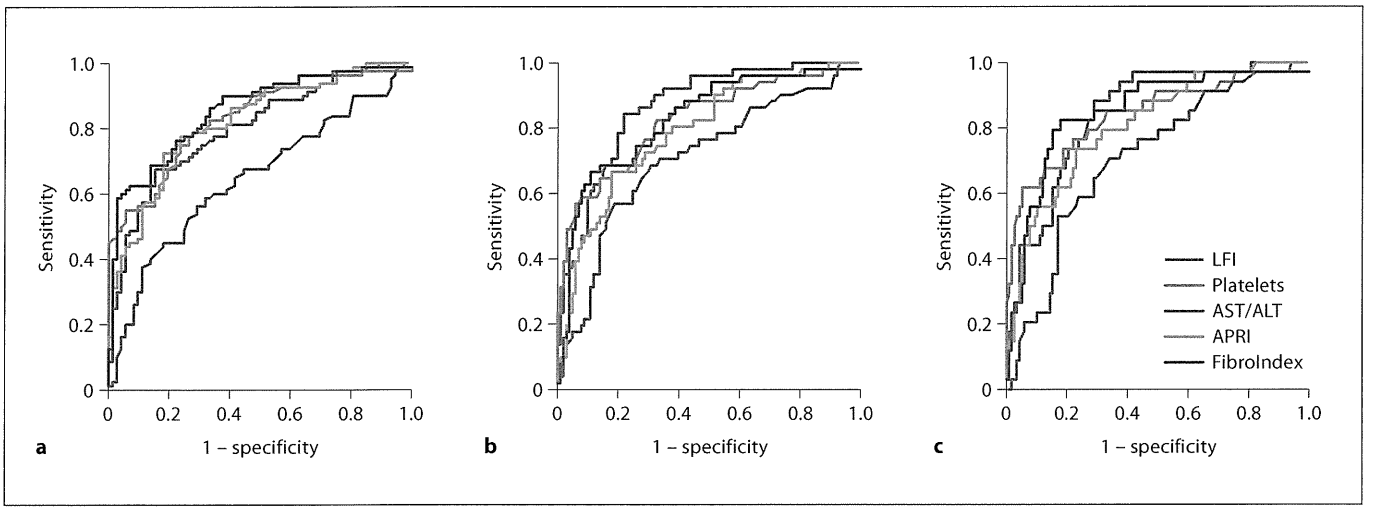

Fig. 3. a ROC curve of the LFI, platelet count, AST/ALT ratio, APRI, and FibroIndex for predicting F2 stage or higher fibrosis (F0–F1 vs. F2–F4). **b** ROC of predicting F3 stage or higher fibrosis. **c** ROC of predicting stage F4 fibrosis.

Table 2. Sensitivity, specificity, positive predictive value, negative predictive value and accuracy of cutoff values of LFI for predicting hepatic fibrosis stage

	Fibrosis stage		
	F0–F1 vs. F2–F4	F0–F2 vs. F3–F4	F0–F3 vs. F4
AUROC	0.800	0.865	0.846
Cutoff value	2.049	2.278	2.357
Sensitivity, %	70.0	78.4	73.5
Specificity, %	76.4	80.2	79.7
Positive predictive value, %	76.7	66.7	51.0
Negative predictive value, %	69.6	88.0	91.3
Accuracy, %	73.0	79.6	78.3

Table 3. AUROC of LFI and several serological makers for predicting liver fibrosis stage

	LFI	Platelets	AST/ALT	APRI	FibroIndex
F0–F1 vs. F2–F4	0.800	0.832	0.646	0.820	0.853
F0–F2 vs. F3–F4	0.865	0.824	0.708	0.789	0.828
F0–F3 vs. F4	0.846	0.840	0.710	0.809	0.850

For diagnosis of cirrhosis (F0–F3 vs. F4), AUROC was 0.846, 0.840, 0.710, 0.809 and 0.850, respectively (table 3, fig. 3). Regardless of the degree of fibrosis progression, RTE has a very good diagnostic capability for liver fibrosis.

Discussion

There is a variety of methods for performing elastography. FibroScan, virtual-touch tissue quantification and shear wave elastography measure the velocity of propagation of the shear wave, which is displayed as elastic modulus or velocity. As the liver becomes hard, the speed of propagation increases. However, the hardness of the liver is also affected by inflammation, jaundice and congestion, as well as fibrosis. FibroScan has been most frequently used in clinical practice to evaluate advanced fibrosis without liver biopsy. However, FibroScan cannot be performed in patients with ascites, narrow intercostal space or severe obesity. Furthermore, it has the disadvantage of low accuracy because there is no B-mode.

RTE displays in real time the relative strain of the tissue by measuring its displacement and does not have the limitations of FibroScan. In the mammary gland, thyroid and prostate, the relative degree of elastic modulus can distinguish malignant space-occupying lesions [13, 14, 20]. As mentioned previously, as liver fibrosis pro-

gresses, the blue portion of the strain image tends to increase in RTE [21]. Shiina et al. [22] have indicated that this pattern of strain images is related to the fibrous structure changes of fibrosis. Several previous studies have focused on the diagnostic accuracy of RTE for liver fibrosis. There are few reports representing a poor accuracy of liver fibrosis. However, the reason for the poor diagnostic accuracy may be the lack of experience of the examiners. To the best of our knowledge, we have been one of the first groups worldwide to perform RTE in patients with liver fibrosis [18, 21, 23, 24]. It is slightly difficult to visualize strain images well. Artifacts such as multiple reflections at the surface of the liver, echo-free areas by thick blood vessels, ribs and lungs, and lack of penetration should be avoided if possible. These are important issues when performing RTE. Although manipulative pressure is used during RTE of the mammary gland and thyroid gland, we performed RTE of the liver without using such pressure. If manipulative pressure is too strong, there is a possibility that the elastic relationship will vary due to the elastic nonlinearity. In addition, there is a possibility that the pressure is not uniformly transmitted to the liver. On the other hand, the liver is deformed slightly by the steady rhythm of the heartbeat. Good images can be obtained merely by light application of the probe to the right intercostal region. Furthermore, because manipulative pressure is not used, human error can be minimized.

LFI in stage F2 fibrosis did not significantly differ from that in stage F3, whereas in all other combinations of stages there were significant differences. The AUROC for prediction of ≥F4 and ≥F2 of LFI was higher than that of serological markers. Our study confirmed that RTE is useful for distinguishing not only advanced fibrosis patients but also mild fibrosis patients from others. Moreover, our study showed that RTE can be performed in all cases, with good discrimination of each fibrosis stage.

In summary, we demonstrated a convenient and noninvasive tool, RTE, for relative strain imaging of the liver. We found that LFI measured by RTE is a useful predictive factor for diagnosis of liver fibrosis stage in patients with chronic viral hepatitis. Our study was based on the gold standard of diagnosis by liver biopsy; therefore, there was a possibility of sampling error. Further studies are desirable on a large number of patients with diagnosis of fibrosis using surgical specimens.

Disclosure Statement

The authors declare that no conflicts of interests exist.

References

1 Nord HJ: Biopsy diagnosis of cirrhosis: blind percutaneous versus guided direct vision techniques – a review. Gastrointest Endosc 1982;28:102–104.
2 Regev A, Berho M, Jeffers LJ, Milikowski C, Molina EG, Pyrsopoulos NT, Feng ZZ, Reddy KR, Schiff ER: Sampling error and intraobserver variation in liver biopsy in patients with chronic HCV infection. Am J Gastroenterol 2002;97:2614–2618.
3 Bedossa P, Dargere D, Paradis V: Sampling variability of liver fibrosis in chronic hepatitis C. Hepatology 2003;38:1449–1457.
4 Joo I, Choi BI: New paradigm for management of hepatocellular carcinoma by imaging. Liver Cancer 2012;1:94–109.
5 Kim DY, Kim SU, Park JY, Ahn SH, Song KJ, Han KH: FibroScan based risk estimation of HBV-related HCC occurrence: development and validation of a predictive model. Liver Cancer 2012;1:123.
6 Sandrin L, Fourquet B, Hasquenoph JM, Yon S, Fournier C, Mal F, Christidis C, Ziol M, Poulet B, Kazemi F, Beaugrand M, Palau R: Transient elastography: a new noninvasive method for assessment of hepatic fibrosis. Ultras Med Biol 2003;29:1705–1713.
7 Friedrich-Rust M, Wunder K, Kriener S, Sotoudeh F, Richter S, Bojunga J, Herrmann E, Poynard T, Dietrich CF, Vermehren J, Zeuzem S, Sarrazin C: Liver fibrosis in viral hepatitis: noninvasive assessment with acoustic radiation force impulse imaging versus transient elastography. Radiology 2009;252:595–604.
8 Ferraioli G, Tinelli C, Dal Bello B, Zicchetti M, Filice G, Filice C: Accuracy of real-time shear wave elastography for assessing liver fibrosis in chronic hepatitis C: a pilot study. Hepatology 2012, E-pub ahead of print.
9 Arena U, Vizzutti F, Corti G, Ambu S, Stasi C, Bresci S, Moscarella S, Boddi V, Petrarca A, Laffi G, Marra F, Pinzani M: Acute viral hepatitis increases liver stiffness values measured by transient elastography. Hepatology 2008;47:380–384.
10 Cobbold JF, Taylor-Robinson SD: Transient elastography in acute hepatitis: all that's stiff is not fibrosis. Hepatology 2008;47:370–372.
11 Millonig G, Reimann FM, Friedrich S, Fonouni H, Mehrabi A, Buchler MW, Seitz HK, Mueller S: Extrahepatic cholestasis increases liver stiffness (FibroScan) irrespective of fibrosis. Hepatology 2008;48:1718–1723.
12 Colli A, Pozzoni P, Berzuini A, Gerosa A, Canovi C, Molteni EE, Barbarini M, Bonino F, Prati D: Decompensated chronic heart failure: increased liver stiffness measured by means of transient elastography. Radiology 2010;257:872–878.
13 Itoh A, Ueno E, Tohno E, Kamma H, Takahashi H, Shiina T, Yamakawa M, Matsumura T: Breast disease: clinical application of US elastography for diagnosis. Radiology 2006; 239:341–350.
14 Fukunari N: More accurate and sensitive diagnosis for thyroid tumors with elastography – detection and differential diagnosis of thyroid cancers. MEDIX Suppl. 2007. http://www.hitachi-medical.co.jp/tech/medix/pdf/supple/sup_05.pdf.

15 Williams AL, Hoofnagle JH: Ratio of serum aspartate to alanine aminotransferase in chronic hepatitis: relationship to cirrhosis. Gastroenterology 1988;95:734–739.
16 Wai CT, Greenson JK, Fontana RJ, Kalbfleisch JD, Marrero JA, Conjeevaram HS, Lok AS: A simple noninvasive index can predict both significant fibrosis and cirrhosis in patients with chronic hepatitis C. Hepatology 2003;38:518–526.
17 Koda M, Matunaga Y, Kawakami M, Kishimoto Y, Suou T, Murawaki Y: FibroIndex, a practical index for predicting significant fibrosis in patients with chronic hepatitis C. Hepatology 2007;45:297–306.
18 Tatsumi C, Kudo M, Ueshima K, Kitai S, Ishikawa E, Yada N, Hagiwara S, Inoue T, Minami Y, Chung H, Maekawa K, Fujimoto K, Kato M, Tonomura A, Mitake T, Shiina T: Non-invasive evaluation of hepatic fibrosis for type C chronic hepatitis. Intervirology 2010;53:76–81.
19 Fujimoto K, Kato M, Tonomura A, Yada N, Tatsumi C, Oshita M, Wada S, Ueshima K, Ishida T, Furuta T, Yamasaki M, Tsujimoto M, Motoki M, Mitake T, Shiina T, Kudo M, Hayashi N: Non-invasive evaluation method of the liver fibrosis using real-time tissue elastograpy: usefulness of judgment liver fibrosis stage by liver fibrosis index (LF index). Kanzo 2010;59:539–541.
20 Miyanaga N, Akaza H, Yamakawa M, Oikawa T, Sekido N, Hinotsu S, Kawai K, Shimazui T, Shiina T: Tissue elasticity imaging for diagnosis of prostate cancer: a preliminary report. Int J Urol 2006;13:1514–1518.
21 Fujimoto K, Wada S, Oshita M, Kato M, Tonomura A, Mitake T: Non-invasive evaluation of hepatic fibrosis in patients with chronic hepatitis C using elastography. MEDIX Suppl. 2007. http://www.hitachi-medical.co.jp/tech/medix/pdf/supple/sup_07.pdf.
22 Shiina T, Maki T, Yamakawa M, Mitake T, Kudo M, Fujimoto K: Mechanical model analysis for quantitative evaluation of liver fibrosis based on ultrasound tissue elasticity imaging. Jpn J Appl Phys 2012; DOI: 10.1143/JJAP.51.07GF11.
23 Morikawa H, Fukuda K, Kobayashi S, Fujii H, Iwai S, Enomoto M, Tamori A, Sakaguchi H, Kawada N: Real-time tissue elastography as a tool for the noninvasive assessment of liver stiffness in patients with chronic hepatitis C. J Gastroenterol 2011; 46:350–358.
24 Tatsumi C, Kudo M, Ueshima K, Kitai S, Takahashi S, Inoue T, Minami Y, Chung H, Maekawa K, Fujimoto K, Akiko T, Takeshi M: Noninvasive evaluation of hepatic fibrosis using serum fibrotic markers, transient elastography (FibroScan) and real-time tissue elastography. Intervirology 2008;51 (suppl 1):27–33.

Reprinted from

JAPANESE JOURNAL OF
APPLIED
PHYSICS

REGULAR PAPER

Mechanical Model Analysis for Quantitative Evaluation of Liver Fibrosis Based on Ultrasound Tissue Elasticity Imaging

Tsuyoshi Shiina, Tomonori Maki, Makoto Yamakawa, Tsuyoshi Mitake, Masatoshi Kudo, and Kenji Fujimoto

Jpn. J. Appl. Phys. **51** (2012) 07GF11

Japanese Journal of Applied Physics 51 (2012) 07GF11 **REGULAR PAPER**
DOI: 10.1143/JJAP.51.07GF11

Mechanical Model Analysis for Quantitative Evaluation of Liver Fibrosis Based on Ultrasound Tissue Elasticity Imaging

Tsuyoshi Shiina, Tomonori Maki, Makoto Yamakawa[1], Tsuyoshi Mitake[2], Masatoshi Kudo[3], and Kenji Fujimoto[4]

Human Health Sciences, Graduate School of Medicine, Kyoto University, Kyoto 606-8507, Japan
[1]*Advanced Biomedical Engineering Research Unit, Kyoto University, Kyoto 606-8501, Japan*
[2]*Hitachi Aloka Medical Ltd., Kashiwa, Chiba 227-0804, Japan*
[3]*Department of Gastroenterology and Hepatology, Kinki University School of Medicine, Osakasayama, Osaka 589-8511, Japan*
[4]*Department of Internal Medicine, National Hospital Organization, Minami-Wakayama Medical Center, Tanabe, Wakayama 646-8558, Japan*

Received November 20, 2011; accepted January 30, 2012; published online July 20, 2012

Precise evaluation of the stage of chronic hepatitis C with respect to fibrosis has become an important issue to prevent the occurrence of cirrhosis and to initiate appropriate therapeutic intervention such as viral eradication using interferon. Ultrasound tissue elasticity imaging, i.e., elastography can visualize tissue hardness/softness, and its clinical usefulness has been studied to detect and evaluate tumors. We have recently reported that the texture of elasticity image changes as fibrosis progresses. To evaluate fibrosis progression quantitatively on the basis of ultrasound tissue elasticity imaging, we introduced a mechanical model of fibrosis progression and simulated the process by which hepatic fibrosis affects elasticity images and compared the results with those clinical data analysis. As a result, it was confirmed that even in diffuse diseases like chronic hepatitis, the patterns of elasticity images are related to fibrous structural changes caused by hepatic disease and can be used to derive features for quantitative evaluation of fibrosis stage. © 2012 The Japan Society of Applied Physics

1. Introduction

Chronic liver damage attributable to hepatitis C virus (HCV) infection results in hepatic fibrosis, which progresses towards cirrhosis, leading to hepatocellular carcinoma, and more than 40,000 people every year die of cirrhosis and hepatic carcinoma in Japan.[1)] Thus, a precise evaluation of the stage of chronic hepatitis C with respect to fibrosis is an important issue to prevent the occurrence of cirrhosis and to initiate appropriate therapeutic intervention such as viral eradication using interferon.[2)]

At present, liver biopsy is still the gold standard for the assessment of liver fibrosis. However, it is an invasive method associated with patient discomfort and, in rare cases, with serious complications.[3,4)] In addition, the accuracy of liver biopsy is limited because of significant intra- and interobserver variability and sampling errors.[5–7)] Therefore, research has been focused on the development of non-invasive methods for the assessment of liver fibrosis.

Diagnostic imaging using B-mode images has been conventionally applied for the diagnosis of liver disease. However, it is not easy to diagnose at its early stage using conventional B-mode images because we have to read subtle changes of speckle patterns, which are not sensitive to the stage of fibrosis.

To overcome this problem, there has been considerable research on quantitative assessment of liver fibrosis based on ultrasonography, such as echo signal processing and texture analysis methods.[8,9)] Yamaguchi and coworkers[10–12)] have recently proposed a method of evaluating the stage of fibrosis using the deviation of echo amplitude distribution from the Rayleigh distribution of a normal liver.

From the viewpoint of directly measuring the stiffness of liver tissue, we investigated the application of tissue elasticity imaging to the evaluation of fibrosis stage. Ultrasonic tissue elasticity imaging can provide us novel diagnostic information based on tissue hardness.[13–15)] Although the first practical system was developed by Shiina *et al.*[13)] for tumor diagnosis, Fujimoto *et al.* have recently reported that the pattern of an elasticity image becomes patchy as fibrosis progresses in the case of diffuse diseases such as chronic hepatitis.[16)] We also proposed the index of liver fibrosis (LF index), which was derived from elasticity images and showed that there was a good correlation between the LF index and the degree of liver fibrosis.[16–18)]

To evaluate fibrosis progression quantitatively on the basis of a strain image, it is important to clarify how fibrosis progression affects the mechanical properties of liver tissues and is consequently expressed in an elasticity image. In this study, we introduced a mechanical model of fibrosis progression and simulated the process by which hepatic fibrosis affects elasticity images and compared the results with clinical data analysis. As a result, it was confirmed that even in diffuse diseases like chronic hepatitis, the pattern of an elasticity image is related to the fibrous structure caused by hepatic disease and can be used to derive features for quantitative evaluation of fibrosis stage.

2. Experimental Methods

2.1 Evaluation of liver fibrosis by ultrasound tissue elasticity imaging

It is well known that chronic liver disease causes hepatic fibrosis, which is characterized by an unusual accumulation of extracellular matrix materials produced by fibroblast-like cells including stellate cells in the hepatic parenchyma. Diagnosing chronic liver disease in the early stage is necessary for the treatment of liver disease because hepatic cirrhosis often leads to other diseases such as liver cancer. In terms of the stage of chronic hepatitis, the new Inuyama scoring system was used, which was proposed by the Japanese Liver Study Group in 1994.[19)] The new Inuyama scoring system classifies chronic hepatitis into five fibrosis stages (F0–F4) on the basis of the extent of the spreading fibrosis and four grades (A0–A3) on the basis of the degree of inflammation and necrosis using liver biopsy samples, as shown in Table I.

Recently, ultrasound systems for the measurement and imaging of tissue elasticity have been developed as noninvasive methods to evaluate the degree of liver fibrosis, providing alternatives to liver biopsy. FibroScan® (transient elastography) detects the propagation speed of a shear wave transmitted from a probe through the liver and calculates the

Table I. New Inuyama scoring system.

Staging (fibrosis)		Grading (necrosis and inflammation)	
F0	No fibrosis	A0	No
F1	Fibrous portal expansion	A1	Mild
F2	Bridging fibrosis	A2	Moderate
F3	Bridging fibrosis with lobular degeneration	A3	Severe
F4	Cirrhosis		

shear modulus of the liver to evaluate the degree of liver fibrosis.[20] Although FibroScan® is simple and easy to use and displays the results on a monitor immediately, it also has many limitations. It cannot be used in patients with narrow intercostal spaces, hepatic atrophy, and ascites since shear waves will not propagate through flues.[21,22] In addition, it is difficult to locally evaluate the degree of fibrosis since the result is based on one-dimensional information (1 line) only.

Ultrasound tissue elasticity imaging is developed for the visual assessment of tissue elasticity, especially for cancer diagnosis. The first practical system was developed by us and employs the algorithm referred to as the combined autocorrelation method proposed by Shiina.[23,24] The method can rapidly calculate a 2-dimensional distribution of tissue deformation, i.e., strain induced by external freehand compression with the probe or by internal heartbeats. In hard tissue, the amount of strain is low, whereas in soft tissue, the amount of strain is higher because soft tissue can be compressed more than hard tissue. However, the strain represents the relative hardness since it changes with compression level. For stable display of the strain distribution free of compression variation, the strain is normalized by the mean value within the region of interest (ROI), ε_0, and displayed with a translucent color superimposed on the B-mode image (soft: red/mean: green/hard: blue), as illustrated in Fig. 1. This method was commercialized in 2003, and referred to as the Real-Time Tissue Elastography® (RTE).[15] At present, several companies have released tissue elasticity imaging systems and different methods for imaging are adopted.

This technology has already been proved to be diagnostically valuable in detecting tumors of the breast, prostate, and other organs.[25] We found that the texture of the elasticity image (strain) of chronic hepatitis becomes a patchy pattern as liver fibrosis progresses and the images could be categorized into the four stages, as shown in Fig. 2.[16,17] The strain induced by heartbeats (diastole) is used to perform RTE. Hepatic fibrosis progresses towards cirrhosis, which causes the fine liver lobule structure to change to a coarse nodular structure stage by stage. The size of the nodules and the volume of the fibers changes with the progression of the disease. Considering this process of fibrosis, it is expected that fibrosis causes inhomogeneous distribution of tissue hardness, which produces a nonuniform texture pattern of strain images.

However, there are limitations to quantitative evaluation of the texture pattern by visual judgement. To increase objectivity, we extract nine image features, as shown in Fig. 3. First of all, the ROI was fixed to a rectangle of about $30 \times 20\,\mathrm{mm}^2$. Pixel data in the colored strain image was

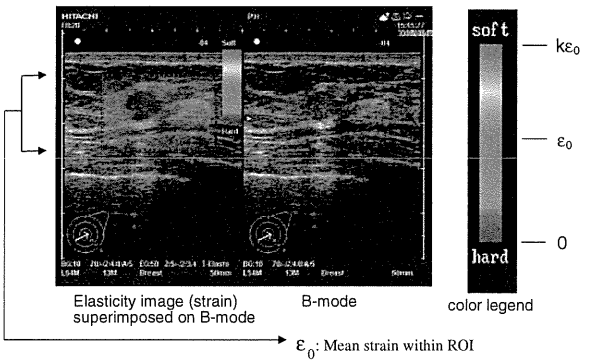

Fig. 1. (Color) Display method of elasticity image.

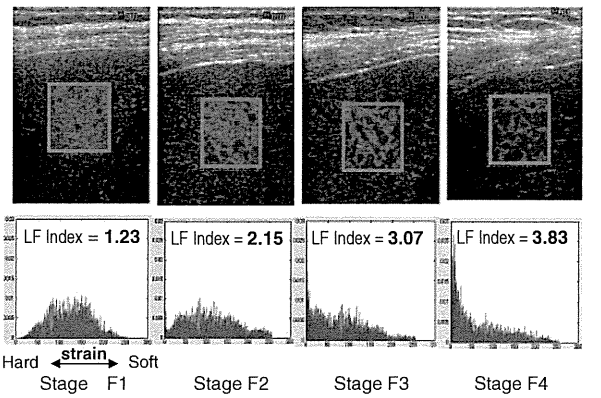

Fig. 2. (Color) Elasticity images (strain) superimposed on B-mode (top) and histogram of the strain distribution within ROI (bottom) for each fibrosis stage of chronic hepatitis.

transformed into a histogram. Finally, we performed multiple regression analysis to derive the LF index in terms of four major features as follows:

$$\text{LF index} = a_1\ \text{MEAN} + a_2\ \text{SD} + a_3\ \%\text{AREA} + a_4\ \text{COMP}. \quad (1)$$

Four major features were defined as follows: MEAN is the mean of the relative (normalized by ε_0) strain value and SD is the standard deviation of the relative strain value, which are calculated from the strain histogram. The strain image is transformed into a binary image, then a blue (or low-strain) area, which indicates a hard area, is detected. %AREA indicates the percentage of the low-strain area or white region in Fig. 3(c) in the ROI. COMP is the complexity of the shape of an extracted low-strain area and is defined by eq. (1),

$$\text{COMP} = \frac{L^2}{S}, \quad (2)$$

where L and S are the boundary length and the area of the low-strain region, respectively.

Thus far, we have performed RTE on 310 cases including 295 patients with chronic hepatitis C and 15 healthy volunteers. As a result, the coefficients of the LF index, $a_1 = -0.00897$, $a_2 = -0.00502$, $a_3 = 0.0232$, and $a_4 =$

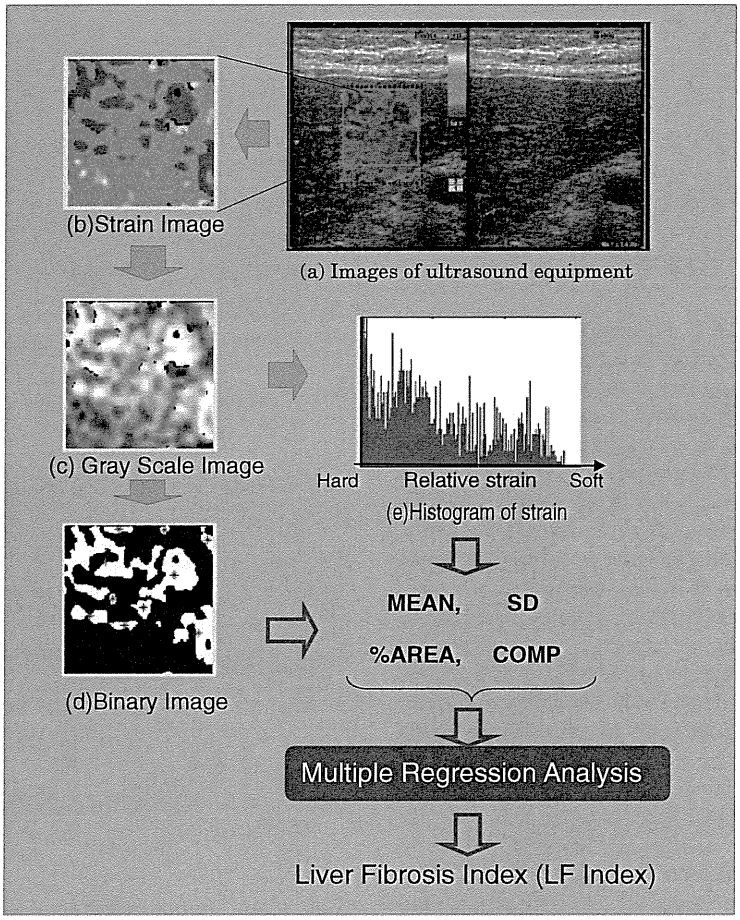

Nine features
1. MEAN : Mean of relative strain value
2. STD : Standard deviation of relative strain value
3. %AREA : Ratio of blue area in analysis region
4. COMP : Complexity of blue area
5. SKEW : Asymmetry of the histogram
6. KURT : Peakedness of the histogram
7. ENT : Textual complexity
8. IDM : Textual local homogeneity (Inverse Difference Moment)
9. ASM :Textual homogeneity (Angular Second Moment)

Fig. 3. (Color) Extraction of image features from strain image and liver fibrosis index (LF index) for quantitative evaluation of fibrosis progression.

0.0253 were obtained. It was confirmed that the LF index highly correlated with the fibrous stage, as shown in Fig. 2.[16)]

2.2 Mechanical model analysis of liver fibrosis

To clarify how fibrosis progression affects the elasticity image of chronic hepatitis, we analyzed the relation by simulating the process with a mechanical model of hepatic fibrosis. At first, the structural changes of liver tissue with fibrous progression are simulated, as shown in Fig. 4. Next, the changes in tissue stiffness and deformation by compression are simulated. Finally, the imaging process and feature extraction by RTE are conducted to compare the results with clinical data.

2.2.1 Modeling of tissue structure changes

The human liver is composed of many hexagonal structures termed liver lobules and containing a central vein. Fibrosis progression is accompanied by changes in tissue structure. When fibrosis progresses, the lobules are destroyed and replaced by regenerative nodules.

In terms of the modeling of the liver tissue structure changes caused by fibrous progression, Yamaguchi *et al.* have carried out much research and proposed a model using the potential distribution.[11)] We referred to the potential distribution model as the initial part to simulate tissue structure changes. In this model, scatterers are distributed densely on the local minimum region of the monomodal potential function as expressed by eq. (3) and

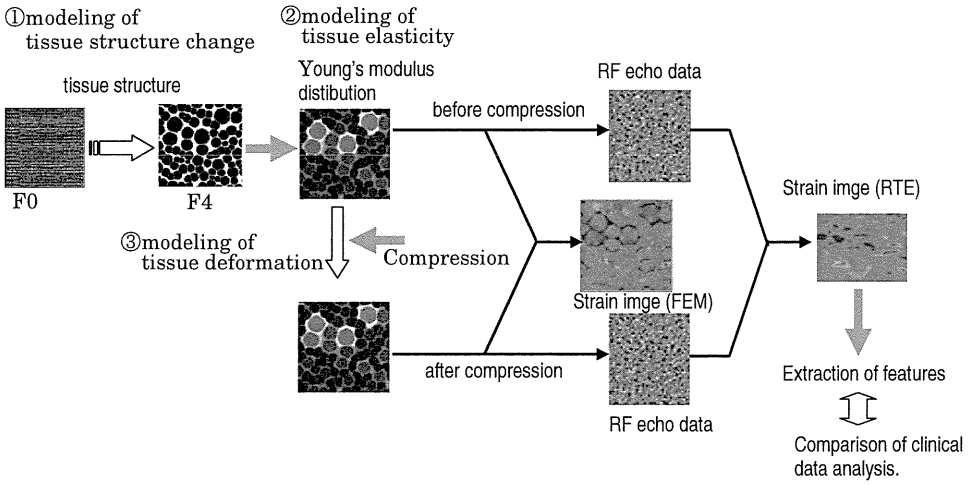

Fig. 4. (Color) Analysis of liver fibrosis progression and its influence on strain imaging using mechanical model.

the position of its peak corresponds to central points of the liver nodule:

$$p(r) = p_{\max} \sin\left(\frac{\pi}{2} k^r\right), \tag{3}$$

where r is the distance from the central point, $p_{\max}$ is the maximal value, and k is the form parameter that determines the distribution spread. The parameter $p_{\max}$ of all the potentials is randomly set to a value from 0.8 to 1.2 as an initial condition and k is set to $0.02 + 0.002 p_{\max}$ as experimentally estimated values as discussed in ref. 11.

To simulate the process by which liver tissue changes from lobules to nodules, the randomly selected central point, r_m, conjugates with its nearest central point, r_n, generating a new central point, r'_m, and a new potential, $p_{\max}(r'_m)$, as follows:

$$r'_m = \frac{\alpha r_n + \beta r_m}{\alpha + \beta}, \tag{4}$$

$$p_{\max}(r'_m) = \alpha + \beta, \tag{5}$$

where $\alpha = p_{\max}(r_m)$, $\beta = p_{\max}(r_n)$.

As a result, fiber tissues generated by conjugation are represented as the minimum region of the potential distribution.

2.2.2 Modeling of tissue elasticity

To simulate tissue deformation, the finite element method (FEM) is applied to the tissue model. For FEM analysis, the ROI ($30 \times 30\,\mathrm{mm}^2$) is divided in a reticular pattern and 500×500 elements; consequently, the element size was $0.06 \times 0.06\,\mathrm{mm}^2$, which can attain the adequate spatial resolution for the strain image. First of all, values of Young's modulus are assigned to each grid point of the structural model in §2.2.1 as follows:

$$E_{\mathrm{p}}(x, y) = \alpha(p_{\max} - \bar{p}_{\max,\mathrm{normal}})^n + E_{\mathrm{normal}} \quad \text{(for parenchyma)}, \tag{6}$$

$$E_{\mathrm{f}}(x, y) = \beta(p_{\mathrm{neighbor,max}} - \bar{p}_{\max,\mathrm{normal}})^n + E_{\mathrm{normal}} \quad \text{(for fibrous region)}, \tag{7}$$

where the parenchyma represents the region of the lobule and nodule except for the fibrous region. $\bar{p}_{\max,\mathrm{normal}}$ is the average of the maximal value of each potential for a normal liver model, and E_{normal} is the average of Young's modulus on the parenchyma of a normal liver model. $p_{\mathrm{neighbor,max}}$ is defined as

$$p_{\mathrm{neighbor,max}} = p_{\max,k} \quad \text{for} \quad \left\{k \mid \max\left(\frac{p_{\max,i}}{d_i^2}\right),\ i = 1, 2, \ldots, M\right\}$$

where $p_{\max,i}$ $(i = 1, 2, \ldots, M)$ are the maximal values of the potential neighbor to the grid point located within the fibrous region and d_i is the distance between the grid point and each central point of the potential.

Here, E_{normal} is set to 4 [kPa] using the values experimentally measured using FibroScan®, as shown in Table II.[26–28] The parameters α and β indicate the contribution ratio of the potential to Young's modulus. The parameter n regulates the rate of stiffness increase, that is, in the case of $n = 1$, E increases in proportion to the conjugated potential, and in the case of $n = 2$, E increases nonlinearly.

Table II. Elastic modulus of liver tissues measured at each fibrous stage. Values in top, middle, and bottom rows are cited from refs. 26, 27, and 28, respectively (unit: kPa).

	F0	F1	F2	F3	F4
Young's modulus[a)]	<5	7	13	18	22
	4.2	6.9	8.9	14.8	26.5
	5.5		6.4	10.0	30.0

a) Measured by FibroScan®.

2.2.3 Modeling of tissue deformation

The Young's modulus distribution model is compressed from the top with a pressure, which causes a slight strain approximately equal to that of clinical examination (about 1%), and the Poisson ratio of the tissue model is set to 0.49. The tissue deformation, that is, the movement of each node of the element, is simulated by FEM assuming the two-dimensional stress state. Displacement of nodes along the axial direction is calculated by comparison of two frame

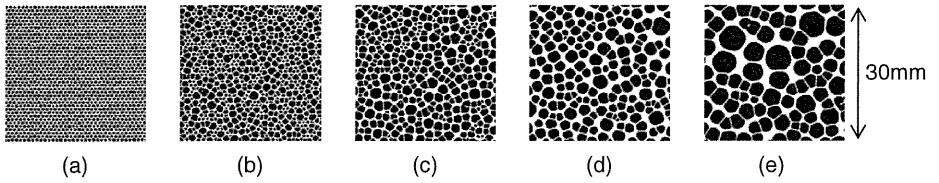

Fig. 5. Simulated tissue structure change caused by the fibrosis progression: (a) stage F0 (Normal): the number of central points is 2538 (the ratio of the number of the central points to that of initial central points is 1), (b) stage F1: 1269 (1/2), (c) stage F2: 635 (1/4), (d) stage F3: 317 (1/8), and (e) stage F4: 159 (1/16).

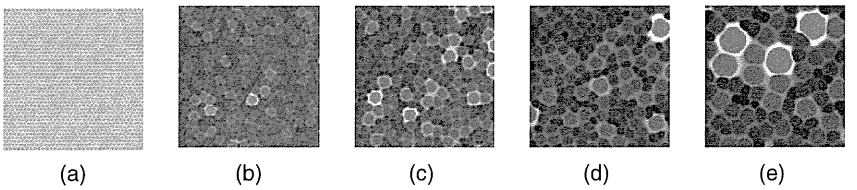

Fig. 6. Young's modulus distribution assigned to tissue structural model: (a) stage F0 (the range of the assigned values of Young's modulus: $E = 0$–5 kPa), (b) stage F1 ($E = 0$–18 kPa), (c) stage F2 ($E = 0$–30 kPa), (d) stage F3 ($E = 0$–72 kPa), and (e) stage F4 ($E = 0$–120 kPa).

data before and after compression. Then, the strain is calculated by differential processing of the displacement. The obtained strain distribution is color-coded and displayed as in RTE.

2.2.4 Feature extraction

For the purpose of evaluating how the tissue stiffness change caused by fibrosis progression is related to the strain distribution, the strain image is directly reconstructed from displacement by FEM analysis in §2.2.3. It is necessary to simulate the signal processing of ultrasound equipment (RTE), since in practice, the strain distribution must be estimated from echo signals.

The number of scatterers distributed within $30 \times 30\,\text{mm}^2$ was set to 4500, that is, the density is 5 points/mm^2 and the scattering coefficient is set on the basis of the tissue structural model. The position of each scatterer after compression is obtained from the position of nodes by FEM analysis. RF echo signals are generated using the transmitted pulse with a Gaussian envelope, a center frequency of 5 MHz, and a duration of 0.4 mm. The beam width is set to 0.8 mm.

Then, the strain distribution is calculated by the combined autocorrelation method and the normalized strain is color-coded as RTE. Finally, four major features were extracted from the strain image and the LF index was calculated to compare the results with clinical cases.

3. Results and Discussion

Figure 5 illustrates the fibrous structures of a normal liver and a liver with chronic hepatitis obtained by modeling of tissue structure change. A two-dimensional model was applied and 2538 central points were distributed within an area ($40 \times 40\,\text{mm}^2$); in other words, liver lobules were located at a mean interval of 0.8 mm. Figure 5(a) presents a normal liver, and Figs. 5(b)–5(e) depict the liver tissue structural changes as fibrosis progresses. The number of iterations does not indicate the physical characteristic of the liver directly, but is selected only to determine the size of nodules. Here, the conjugation process was repeated until the number of central points reduced to 1/2 (for stage F1), 1/4 (F2), 1/8 (F3), and 1/16 (F4) of the initial central points simply assuming that the average numbers of conjugations are 1, 2, 3, and 4, for each stage. We can observe that the sizes of the nodules and the widths of the fibers increase with the progression of liver fibrosis and inhomogeneous structures are also evident in serious cases.

Table III. Comparison of elastic modulus between model and measured values (unit: kPa).

	F0	F1	F2	F3	F4
Mean values of Young's modulus set to the model	4.0	6.2	10.0	17.1	35.7
Young's modulus[a)]	4.9	6.5	9.4	14.3	26.2

a) Measured by FibroScan®. Averaged values from refs. 26–28.

Figure 6 illustrates the Young's modulus distribution assigned to the models in Fig. 5. The range of Young's modulus values for each image is indicated at the Fig. 6 legend. The parameters in eqs. (6) and (7) were set to $n = 1$ and $\alpha = \beta = 1.3$, so that the mean values of Young's modulus assigned for each stage were close to the values measured by FibroScan®, as shown in Table III.

As fibrosis progresses, the maximum potential $p_{\max}$ becomes higher, so the assigned values of Young's modulus $E(x, y)$ increase accordingly owing to eqs. (5) and (6). As a result, it can be seen that the region around a large nodule has large values of Young's modulus in Fig. 6, namely, it becomes hard.

The tissue model shown in Fig. 6 was compressed from the top by applying 50 Pa (1.25% of $E_{\text{normal}} = 4$ kPa) in the axial direction. Then, strain images were obtained, as shown in Fig. 7. The top images are strain images reconstructed directly from the displacement obtained by FEM analysis. The bottom images are estimated from the echo signals

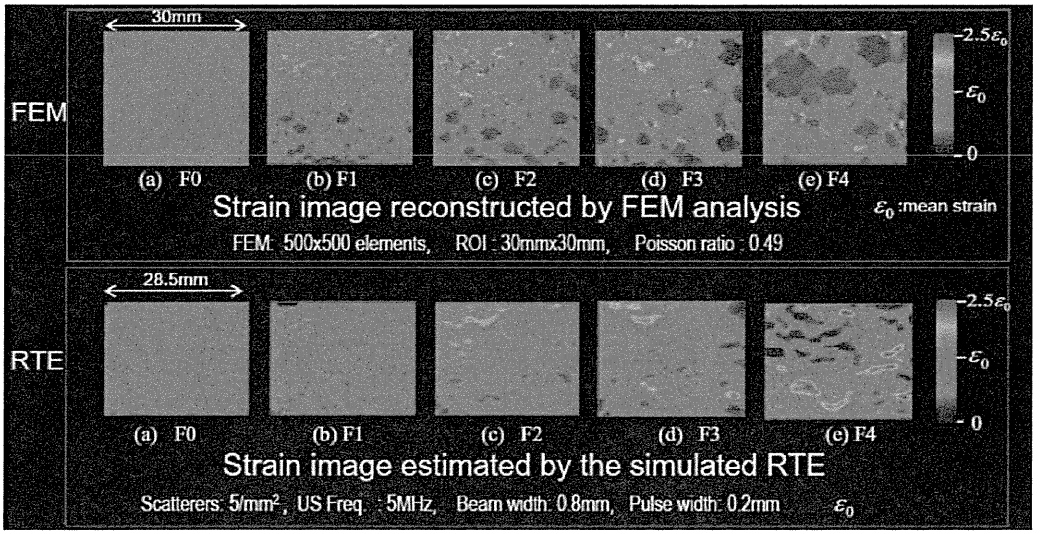

Fig. 7. (Color) Strain images obtained by FEM analysis and simulated RTE.

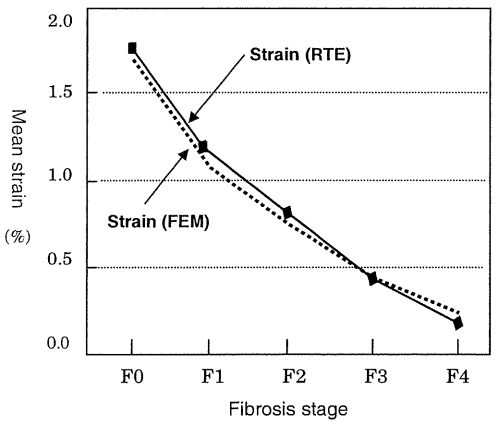

Fig. 8. Change in mean values of strain images.

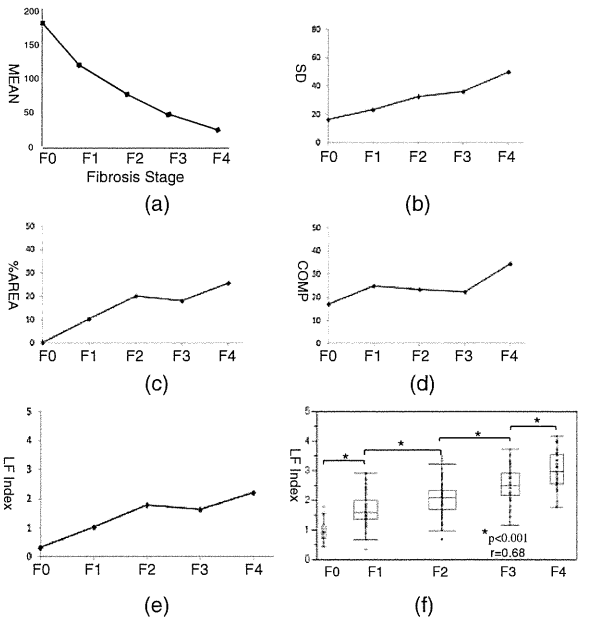

Fig. 9. Features of strain image and LF index as a function of fibrosis stage in the case of $n = 1$, and $\alpha = \beta = 1.3$ [parameters in eqs. (6) and (7)]: (a) MEAN, (b) SD, (c) %AREA, (d) COMP, (e) LF index, and (f) the relationship of LF index and fibrosis stage obtained by clinical data analysis for 310 cases.

generated by simulating RTE. Compared with the strain image obtained by FEM, the display area of the strain image obtained by RTE is smaller ($28.5 \times 21.6\,\mathrm{mm}^2$) since marginal parts are used for estimation. It can be seen that, as fibrosis progresses, the blue area increases, indicating that the area has become stiffer than the area around it. In addition, the strain distribution becomes increasingly complex.

Figure 8 represents the mean strain within the analyzed area for each stage. We can see that the mean strain decreases as the stage progresses. It should be noted that strain images obtained by FEM reflect the pattern of Young's modulus distribution in Fig. 6. In addition, there is naturally a good correlation between both strain images although strain images obtained by RTE are more blurred than those obtained by FEM since the former are estimated from echo signals.

Finally, four features extracted from the strain image (RTE) and LF index derived using eq. (1) as a function of fibrosis stage are shown in Fig. 9. For the simulation in Figs. 9(a)–9(e), the parameter n in eq. (6) was set to 1 as well as in Figs. 6 and 7. It can be observed that MEAN decreases, while SD and %AREA increase as fibrosis progresses. COMP seems to become large in serious cases. As shown in Fig. 9(e), the LF index derived from these features also tends to increase. The relationship between the LF index and fibrosis stage obtained by clinical data analysis of the 310 cases is shown in Fig. 9(f). Although the result of

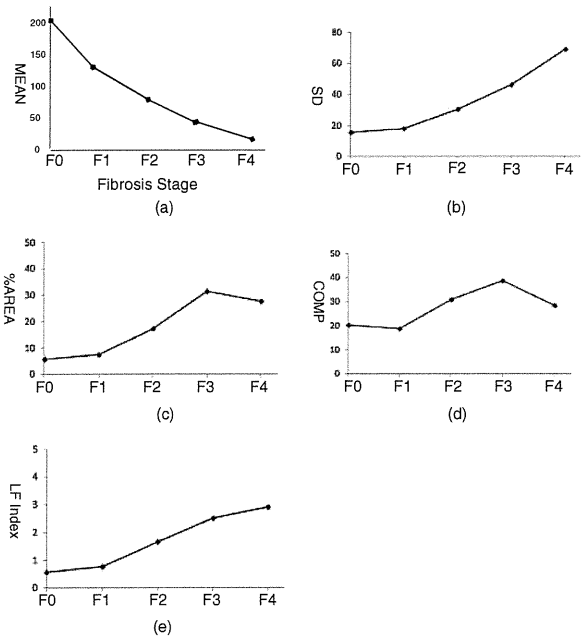

Fig. 10. Features of strain image and LF index as a function of fibrosis stage in the case of $n = 2$, and $\alpha = \beta = 0.1$ [parameters in eqs. (6) and (7)]: (a) MEAN, (b) SD, (c) %AREA, (d) COMP, and (e) LF index.

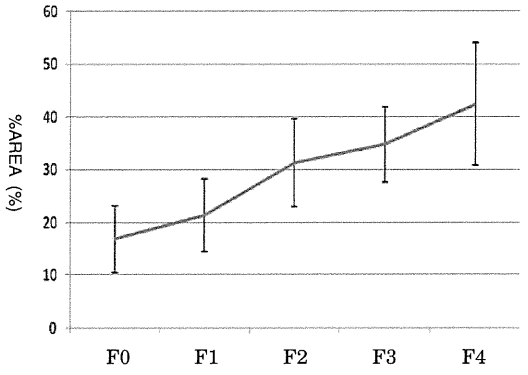

Fig. 11. Change in %AREA as a function of fibrosis stage (clinical data analysis).

simulation analysis is for a single case, the LF index obtained using a mechanical model of fibrosis progression coincides with the result of the clinical data analysis.

These results indicate that even in diffuse diseases like chronic hepatitis, the pattern of strain images is related to the fibrous structure changes caused by hepatic disease and can be used to derive features for quantitative evaluation of fibrosis stage.

On the other hand, there remain several problems to be solved for the development of a clinically useful method. For example, the parameters of models described in §2.2.1 and §2.2.2 are defined only to determine the size of the nodules or the rate of stiffness increase. Therefore, they do not directly indicate the physical characteristic of the liver. In particular, the number of iterations is an important parameter, although there is no *a priori* information at present. In terms of the parameter n, representing the rate of stiffness increase, if parameters are set to $n = 2$ and $\alpha = \beta = 0.1$, the staging is accelerated, as shown in Fig. 10. To tune or optimize these parameters, it is indispensable to continue the simulation under several conditions and compare the results with a large number of clinical data.

As mentioned in §2.1, chronic hepatitis is scored by fibrosis staging and grading. Our clinical research validates that the LF index obtained by RTE stably reflects the fibrosis stage without being influenced by variables of inflammatory state or blood pressure. On the other hand, it is reported that the values measured by FibroScan® are influenced by variables such as hepatic steatosis and flares of transaminases.[21,22] This indicates that shear wave velocity is also changed by factors other than fibrosis stage. In terms of shear wave velocity measurement, some methods using acoustic radiation force for shear wave generation within the body have been recently developed such as acoustic radiation force impulse (ARFI) imaging[29] and shear wave elastography (SWE).[30] These methods can also be used as noninvasive methods of assessing tissue stiffness. In addition, it is expected to utilize different diagnosis information by using both methods, that is, strain image and shear wave image.

4. Conclusions

In this study, we proposed a mechanical model of fibrosis progression. From the strain distribution, we could see that the area of low strain increases, and the strain distribution becomes increasingly complex as fibrosis progresses. The extracted features of strain and derived the LF liver index showed a definite correlation with fibrosis progression and coincided with the result of clinical data analysis. This indicates that even in diffuse diseases like chronic hepatitis, the pattern of strain images is related to the fibrous structure changes caused by hepatic disease and can be used to derive features for quantitative evaluation of fibrosis stage.

As mentioned above, to optimize the parameters used for simulation analysis, it is indispensable to continue the simulation under several conditions and compare the results with a large number of clinical data. For example, although the number of iterations for the conjugating process does not directly indicate the physical characteristic of the liver, the %AREA may be a useful reference to relate the number of iterations to the fibrosis stages. Figure 11 shows the %AREA obtained by clinical data analysis, which increases as a function of fibrosis stage and is similar to Fig. 9(c).

In addition, for future work, there remain some problems to be investigated. To extract reliable diagnosis information from a strain image, a stable data acquisition system that is robust against noise and artifacts must be developed. To improve the precision of simulation, we must investigate a way to obtain the precise values of Young's modulus for each component, such as the parenchyma and fibrous portion, for example, by microscopic measurement of tissues for each stage of hepatitis. Finally, in terms of the extraction of image features, it is one of the most important themes of this research to extract more appropriate features to be useful for the precise diagnosis of chronic hepatitis.

1) A. Ohshima: Proc. 123rd Symp. Japanese Association of Medical Sciences, 2003, p. 13 [in Japanese].
2) National Institutes of Health Consensus Development Conference Statement. Management of Hepatitis C: Hepatology **36** (2002) S3.
3) A. A. Bravo, S. G. Sheth, and S. Chopra: New Engl. J. Med. **344** (2001) 495.
4) I. Sporea, A. Popescu, and R. Sirli: World J. Gastroenterol. **14** (2008) 3396.
5) P. Bedossa, D. Dargère, and V. Paradis: Hepatology **38** (2003) 1449.
6) M. Ziol, A. Handra-Luca, A. Kettaneh, C. Christidis, F. Mal, F. Kazemi, V. de Ledinghen, V. P. Marcelin, D. Dhumeaux, J. C. Trinchet, and M. Beaugran: Hepatology **41** (2005) 48.
7) U. Arena, F. Vizzutti, G. Corti, S. Ambu, C. Stasi, S. Bresci, S. Moscarella, V. Boddi, A. Petrarca, G. Laffi, F. Marra, and M. Pinzani: Hepatology **47** (2008) 380.
8) Y. Fujii, N. Taniguchi, and K. Itho: Med. Imaging Technol. **21** (2003) 117.
9) T. Nishimura, H. Watanabe, M. Ito, Y. Matsuoka, K. Yano, M. Daikoku, H. Yaysuhasshi, K. Dohmen, and H. Ishibashi: Br. J. Radiol. **78** (2005) 189.
10) T. Yamaguchi, H. Hachiya, K. Kato, H. Fukuda, and M. Ebara: Jpn. J. Appl. Phys. **39** (2000) 3266.
11) T. Yamaguchi, K. Nakamura, and H. Hachiya: Jpn. J. Appl. Phys. **42** (2003) 3292.
12) Y. Igarashi, H. Ezuka, T. Yamaguchi, and H. Hachiya: Jpn. J. Appl. Phys. **49** (2010) 07HF06.
13) T. Shiina, N. Nitta, E. Ueno, and J. C. Bamber: J. Med. Ultrason. **29** (2002) 119.
14) M. Yamakawa, N. Nitta, T. Shiina, M. Matsumura, S. Tamano, T. Mitake, and E. Ueno: Jpn. J. Appl. Phys. **42** (2003) 3265.
15) A. Itoh, E. Ueno, E. Tohno, H. Kamma, H. Takahashi, T. Shiina, M. Yamakawa, and T. Matsumura: Radiology **231** (2006) 341.
16) K. Fujimoto, M. Kato, A. Tonomura, N. Yada, C. Tatsumi, M. Oshita, S. Wada, K. Ueshima, T. Ishida, T. Furuta, M. Yamasaki, M. Tsujimoto, M. Motoki, T. Mitake, S. Kim, K. Yamamoto, T. Shiina, M. Kudo, and N. Hayashi: Kanzo **51** (2010) 539 [in Japanese].
17) A. Tonomura, M. Motoki, T. Mitake, K. Fujimoto, M. Kato, C. Tatsumi, N. Yada, K. Ueshima, M. Kudo, and T. Shiina: Proc. 22nd Kanto-section Meet. JSUM, 2010, p. 36 [in Japanese].
18) C. Tatsumi, M. Kudo, K. Ueshima, S. Kitai, E. Ishikawa, N. Yada, S. Hagiwara, T. Inoue, Y. Minami, H. Chung, K. Maekawa, K. Fujimoto, M. Kato, A. Tonomura, T. Mitake, and T. Shiina: Intervirology **53** (2010) 76.
19) F. Ichida, T. Tsuji, M. Omata, T. Ichida, K. Inoue, T. Kaminuma, G. Yamada, K. Hino, O. Yokosuka, and H. Suzuki: Int. Hepatol. Commun. **36** (1996) 112.
20) L. Sandrin, B. Fourquet, J. M. Hasquenoph, S. Yon, C. Fournier, F. Mal, C. Christidis, M. Ziol, B. Poulet, F. Kazemi, M. Beaugrand, and R. Palau: Ultrasound Med. Biol. **29** (2003) 1705.
21) M. Friedrich-Rust, M. F. Ong, S. Martens, C. Sarrazin, J. Bojunga, S. Zeuzem, and E. Herrmann: Gastroenterology **134** (2008) 960.
22) U. Arena, F. Vizzutti, G. Corti, S. Ambu, C. Stasi, S. Bresci, S. Moscarella, V. Boddi, A. Petrarca, G. Laffi, F. Marra, and M. Ponzani: Hepatology **47** (2008) 380.
23) T. Shiina, M. M. Doyley, and J. C. Bamber: Proc. IEEE Ultrasonics Symp., 1996, 1331.
24) M. Yamakawa and T. Shiina: Jpn. J. Appl. Phys. **40** (2001) 3872.
25) E. Tohno and E. Ueno: Breast Cancer **15** (2008) 200.
26) National Center for Global Health and Medicine, Disease Control and Prevention Center (2008) [http://www.ncgm.go.jp/center/formedsp_cir.html] [in Japanese].
27) T. Yasuda, T. Takeda, Y. Nakayama, K. Uehata, H. Sakaguchi, M. Seki, A. Sawada, M. Yamashita, K. Abo, S. Takeda, and H. Asai: presented at 151st Osaka Abdomen Ultrasound, 2005 [in Japanese].
28) M. Ziol, A. Handra-Luca, A. Kettaneh, C. Christidis, F. Mal, F. Kazemi, V. de Lédinghen, P. Marcellin, D. Dhumeaux, J. C. Trinchet, and M. Beaugrand: Hepatology **41** (2005) 48.
29) M. L. Palmeri, M. H. Wang, J. J. Dahl, K. D. Frinkley, and K. R. Nightingale: Ultrasound Med. Biol. **34** (2008) 546.
30) J. Bercoff, M. Tanter, and M. Fink: IEEE Trans. Ultrason. Ferroelectr. Freq. Control **51** (2004) 396.

J Gastroenterol (2012) 47:444–451
DOI 10.1007/s00535-011-0505-8

ORIGINAL ARTICLE—LIVER, PANCREAS, AND BILIARY TRACT

Decrease in alpha-fetoprotein levels predicts reduced incidence of hepatocellular carcinoma in patients with hepatitis C virus infection receiving interferon therapy: a single center study

Yukio Osaki · Yoshihide Ueda · Hiroyuki Marusawa · Jun Nakajima · Toru Kimura · Ryuichi Kita · Hiroki Nishikawa · Sumio Saito · Shinichiro Henmi · Azusa Sakamoto · Yuji Eso · Tsutomu Chiba

Received: 28 July 2011 / Accepted: 24 October 2011 / Published online: 23 November 2011

Abstract
Background Increasing evidence suggests the efficacy of interferon therapy for hepatitis C in reducing the risk of hepatocellular carcinoma (HCC). The aim of this study was to identify predictive markers for the risk of HCC incidence in chronic hepatitis C patients receiving interferon therapy.
Methods A total of 382 patients were treated with standard interferon or pegylated interferon in combination with ribavirin for chronic hepatitis C in a single center and evaluated for variables predictive of HCC incidence.
Results Incidence rates of HCC after interferon therapy were 6.6% at 5 years and 13.4% at 8 years. Non-sustained virological response (non-SVR) to antiviral therapy was an independent predictor for incidence of HCC in the total study population. Among 197 non-SVR patients, independent predictive factors were an average alpha-fetoprotein (AFP) integration value $\geq$10 ng/mL and male gender. Even in patients whose AFP levels before interferon therapy were $\geq$10 ng/mL, reduction of average AFP integration value to <10 ng/mL by treatment was strongly associated with a reduced incidence of HCC. This was significant compared to patients with average AFP integration values of $\geq$10 ng/mL ($P = 0.009$).
Conclusions Achieving sustained virological response (SVR) by interferon therapy reduces the incidence of HCC in hepatitis C patients treated with interferon. Among non-SVR patients, a decrease in the AFP integration value by interferon therapy closely correlates with reduced risk of HCC incidence after treatment.

Keywords Alpha-fetoprotein · Hepatocellular carcinoma · Hepatitis C · Interferon

Y. Osaki · J. Nakajima · T. Kimura · R. Kita · H. Nishikawa · S. Saito · S. Henmi · A. Sakamoto · Y. Eso
Department of Gastroenterology and Hepatology, Osaka Red Cross Hospital, 5-53 Fudegasaki-cho, Tennoji-ku, Osaka 543-8555, Japan

Y. Ueda (✉) · H. Marusawa · Y. Eso · T. Chiba
Department of Gastroenterology and Hepatology, Graduate School of Medicine, Kyoto University, 54 Kawahara-cho, Shogoin, Sakyo-ku, Kyoto 606-8507, Japan
e-mail: yueda@kuhp.kyoto-u.ac.jp

Introduction

Hepatitis C virus (HCV) infection is a predominant cause of liver cirrhosis and hepatocellular carcinoma (HCC) in many countries, including Japan, the United States, and countries of Western Europe [1–5]. The annual incidence of HCC in patients with HCV-related cirrhosis ranged from 1 to 8% [6–9]. Even in the absence of liver cirrhosis, patients with chronic hepatitis caused by HCV infection are at a high risk of developing HCC. Indeed, a large-scale Japanese cohort study showed that the annual incidence of HCC is 0.5% among patients with stage F0 or F1 fibrosis and 2.0, 5.3, and 7.9% among those with F2, F3, and F4 fibrosis, respectively [9]. Periodic surveillance is recommended to detect HCC as early as possible in patients with HCV-related chronic liver disease; however, this may not be cost-effective. For patients with chronic hepatitis C, more effective detection and prevention of HCC is being sought by two important routes: (1) the attempt to discover noninvasive predictive markers and (2) development of treatment strategies to reduce the risk of HCC. There have been several attempts to discover non-invasive markers capable of predicting the risk of HCC incidence in patients with chronic hepatitis C [6, 10]. For example, a cohort